Available online at www.sciencedirect.com
ScienceDirect
Biochimica et Biophysica Acta 1767 (2007) 484–492
Biochimica et Biophysica Acta
BBA
www.elsevier.com/locate/bbabio

Review

Mono-manganese mechanism of the photosytem II water splitting reaction by a unique Mn_4Ca cluster

Masami Kusunoki *

Department of Physics, School of Science and Technology, Meiji University, Tama-ku, Kawasaki, Kanagawa, 214-8571, Japan

Received 24 November 2006; received in revised form 19 March 2007; accepted 27 March 2007
Available online 4 April 2007

Abstract

The molecular mechanism of the water oxidation reaction in photosystem II (PSII) of green plants remains a great mystery in life science. This reaction is known to take place in the oxygen evolving complex (OEC) incorporating four manganese, one calcium and one chloride cofactors, that is light-driven to cycle four intermediates, designated S_0 through S_4, to produce four protons, five electrons and lastly one molecular oxygen, for indispensable resources in biosphere. Recent advancements of X-ray crystallography models established the existence of a catalytic Mn_4Ca cluster ligated by seven protein amino acids, but its functional structure is not yet resolved. The ^{18}O exchange rates of two substrate water molecules were recently measured for four S_i-state samples ($i=0$–3) leading to $^{34}O_2$ and $^{36}O_2$ formations, revealing asymmetric substrate binding sites significantly depending on the S_i-state. In this paper, we present a chemically complete model for the Mn_4Ca cluster and its surrounding enzyme field, which we found out from some possible models by using the hybrid density functional theoretic geometry optimization method to confirm good agreements with the 3.0 Å resolution PSII model [B. Loll, J. Kern, W. Saenger, A. Zouni , J. Biesiadka, Nature 438 (2005) 1040–1044] and the S-state dependence of ^{18}O exchange rates [W. Hillier and T. Wydrzynski, Phys. Chem. Chem. Phys. 6 (2004) 4882–4889]. Furthermore, we have verified that two substrate water molecules are bound to asymmetric cis-positions on the terminal Mn ion being triply bridged (μ-oxo, μ-carboxylato, and a hydrogen bond) to the $Mn_3CaO_3(OH)$ core, by developing a generalized theory of ^{18}O exchange kinetics in OEC to obtain an experimental evidence for the cross exchange pathway from the slow to the fast exchange process. Some important experimental data will be discussed in terms of this model and its possible tautomers, to suggest that a cofactor, Cl^- ion, may be bound to CP43-Arg357 nearby Ca^{2+} ion and that D1-His337 may be used to trap a released proton only in the S_2-state.

Keywords: Photosynthesis; Photosystem II; Oxygen evolution; Water oxidation; Manganese cluster; DFT B3LYP method; Tautomerism; Manganese EPR; Water exchange kinetics

1. Introduction

The water-splitting and oxygen-evolving reaction in plant PSII would be one of the most fundamental and the most important photochemical reactions for all lives on the earth. This enzyme reaction for substrate water molecules, from which electrons and protons are decomposed to evolve dioxygen, is considered to take place in a unique Mn_4Ca cluster placed in a special enzyme field, undergoing a cyclic change of redox intermediate states, designated "S_i-states" ($i=0$, 1, 2, 3,4) [1]. The driving force for this reaction is subsequently created as an oxidized species of a neighboring Tyr161, denoted $Y_Z^{\bullet}$, with its phenol proton being dislocated to H190. [2,3] In recent 5 years, the X-ray crystallography approach have elucidated the atomic structure of the OEC in PS II, with an increasing resolution of 3.8 Å [4], 3.7 Å [5], 3.5 Å [6], 3.2 Å [7,8] and 3.0 Å [8]. Especially, at 3.5 Å resolution, J. Barber' group [6] proposed a detailed model for the Mn_4Ca cluster, which contains a cubane-like Mn_3CaO_4 core joining a fourth Mn ion by a μ_4-oxo bridge, and binds two substrate water molecules on Ca^{2+} and the 4th Mn ion each, to propose a "nucleophilic attack" mechanism of the O–O bond formation. This so-called London model has greatly inspired quantum chemists to enter this challenging field [9,10]. However, at improved 3.0 Å resolution in an optimized condition to suppress radiation-damage, Loll et al. [8] suggested an alternative OEC structure, called "Berlin model", which

* Tel: +86 44 934 7433; fax: +86 44 934 7911.
E-mail address: kusunoki@isc.meiji.ac.jp.

0005-2728/$ - see front matter © 2007 Elsevier B.V. All rights reserved.
doi:10.1016/j.bbabio.2007.03.012

contains an MT-type Mn_4Ca core ligated by six carboxylate groups and an imidazole group in two proteins.

So far, the skeleton structure and the oxidation state of four Mn ions in OEC has been extensively studied mainly by using Mn K-edge X-ray absorption fine structure (XAFS) spectroscopy [11–17], and electron paramagnetic resonance (EPR) spectroscopy [18–24]. Early observations of Mn K-edge extended XAFS (EXAFS) from PSII samples poised in S_1 [25] and in S_1 and S_2 [26] revealed the existence of short (~2.7 Å) and long (~3.3 Å) Mn–Mn distances in the cluster. This led to a dimer of dimers (DD) model in which two di-μ_2-oxo bridged Mn–Mn dimers are connected by a mono-μ_2-oxo bridge [27]. On the other hand, the quantum mechanical theory developed to explain the S_2-state multiline signal (MLS) at $g=2$ [28] was applied to revealing the structure of manganese spin-exchange interactions ($\Sigma_{(i>j)}J_{ij}S_i\cdot S_j$; $i, j=a-d$) and the manganese spin hamiltonians in S_2 state. This computational search was carried out for the paramagnetic S_2 state that is characterized by the spin $S=1/2$ ground state accompanying the first excited state at ~20–50 cm^{-1}, as well as the effective ^{55}Mn hyperfine coupling (hfc) tensors $\{\boldsymbol{A}_i: i=a-d\}$ determined from oriented MLS at X-band frequency [29–31]. Thus, a conclusion was derived that the most promising cluster would be a MT-type of dislocated cubane, in which only one strong anti-ferromagnetic interaction between Mn(III) and Mn(IV) spins (~230–300 cm^{-1}) and at most two intermediate interaction(s) must exist in the T part. Incidentally, the ESE_ENDOR (Electron Spin Echo Electron and Nuclear Double Resonance) spectroscopy [32] was applied to this EPR signal to make a small correction only to the smallest hfs tensor. In real enzyme, two or more ligand(s) might serve as bridges between M and T, to induce one (J_{ab}) or two (J_{ab}/J_{ac}) spin-exchange interaction(s). In the former case, this $Mn–Mn_3$ cluster may be called "MT-4J type" (e.g. "dangler model" [32]), and in the latter case, this is called "MT-5J type" (e.g. "diamond-structure model" [33–35] and "London model" [6]), since the T part contains three spin-exchange interactions (J_{bc}, J_{bd}, J_{cd}). In the MT-type dangler model, M and T may be linked either by a mono-μ_2-oxo bridge or mono-μ_2-oxo-mono-μ_2-carboxylato bridges, to induce a weak-antiferromagnetic or weak-ferromagnetic J_{ab}. In the MT-type London model, M and T are supposed to be connected by a μ_4-oxo bridge, which may induce two small spin-exchange interactions, J_{ab} and J_{ac}. But, when M and T are strong-antiferromagnetically linked by di-μ_2-oxo-bridges as in models [36,37], the Mn_4Ca cluster will be called "T-shaped DD (TDD)" model to distinguish it from the previous MT-type.

On the other hand, some attempts to monitor the substrate–water (or its derivative) binding in the Mn_4Ca cluster has been made using the proton release kinetics [38,39], the electron and nuclear paramagnetic resonances [40,41], the ^{18}O exchange kinetics for the substrate water in PSII [42], and the isotope labeled FTIR [43,44] measurements. Especially, the ^{18}O exchange kinetics determined by time-resolved mass spectroscopic methods has provided the most direct information on the chemical nature of the substrate binding sites in OEC [42]. The kinetic data for $^{34}O_2$ and $^{36}O_2$ yields have been taken as evidence for the separate substrate binding sites, as illustrated in Fig. 1A, based on the eye-measurement separation of the slow and fast exchange processes for two substrates [42]. However, to abstract the precise information on the nature of the binding sites, we have developed a generalized theory of ^{18}O exchange reaction kinetics taking into account the cross exchange pathways between the transition states in slow and fast exchange processes. In Section 2.3, this theory will be applied to the most reliable S_1-state data, concluding that the two substrate water molecules are most probably bound to *cis*-positions of the same Mn ion with different binding affinities, as illustrated in Fig. 1B.

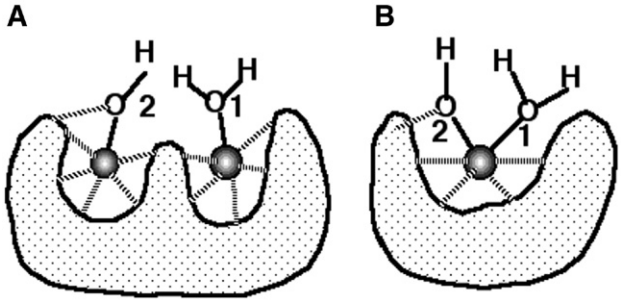

Fig. 1. Two possible models for two substrate water (or its derivative) binding sites in the Mn_4Ca cluster in OEC: (A) bi-metallic vs. (B) mono-metallic. Note that this topological classification will be used as the functional classification of "independent" vs. "correlated", respectively. Water 2 is supposed to be more strongly bound than water 1 by the intrinsic chemical bond itself and/or an intra-cluster hydrogen bond (a ladder line).

In this paper, it will be shown that the EPR-favorable MT-5J type dislocated cubane model could lead to the most likely complete structure of the Mn_4Ca cluster in OEC through some theoretical critical usages of reported kinetic and spectroscopic data described above.

2. How to predict the structure of the Mn_4Ca cluster

2.1. Hybrid density functional theory method

The molecular structures of model Mn_4Ca clusters have been optimized by the standard DFT/B3LYP method with use of a double-ζ quality basis set, lavcp**, which can predict the geometries of multinuclear manganese complexes within an accuracy of ~0.02 Å [45], but, the SCF energies have been calculated only for the high-spin states with use of a triple-ζ quality basis set, lavc3p**, to keep the best accuracy (~3 kcal/mol) of the relative energy levels; both in the default setting of Jaguar 5.1 [46].

2.2. Oxidation states and electronic spins of four manganese ions

Hitherto, the oxidation state of the Mn_4Ca cluster has been extensively studied by means of Mn-EPR and Mn K-edge XAFS spectroscopies. But, plural models are still asserted: i.e. (3III,IV) [11] or (II,III,2IV) [17,47] or (II,3III) [48,49] in S_0; (2III,2IV) [11,17,47] or (4III) [48,49] in S_1; (III,3IV) [11,17,47] or (3III, IV) [48–50] in S_2; and (4IV) [11,17] or (III,3IV) [47,51] or (2III,2IV) [48,49] in S_3, where our model is written in the first. Our model will be supported by results to be presented.

2.3. A generalized theory of ^{18}O–substrate exchange kinetics in OEC

In Fig. 2, we depict a generalized scheme of $^{16}O/^{18}O$ exchange reaction kinetics for two substrate water molecules bound to the Mn_4Ca cluster (M). The superfix and suffix positions in M^{α}_{β} represent a weak and strong substrate binding sites, respectively, and α and β represent ^{16}O- and ^{18}O-substrate molecule, respectively. The fast, slow, forward-cross and backward-cross exchange rates are denoted k_1, k_2, k_3 and k_{-3}, respectively. When the ^{18}O enrichment was set to ε ($0<\varepsilon<1$) at $t=0$, the normalized yields of isotopes, $^{34}O_2$ and $^{36}O_2$, at injection time t are respectively given by

$$^{34}Y(t) = (\kappa/2)[(1+\tilde{x}_{-3})\{1+A^{\alpha}_{\beta}e^{-k_1 t} - B^{\alpha}_{\beta}e^{-K_2 t} - (1+A^{\alpha}_{\beta} - B^{\alpha}_{\beta})e^{-(k_1+K_2)t}\} + (1+\tilde{x}_3)\{1+A^{\beta}_{\alpha}e^{-k_1 t} - B^{\beta}_{\alpha}e^{-k_2 t} - (1+A^{\beta}_{\alpha} - B^{\beta}_{\alpha})e^{-(K_1+k_2)t}\}], \quad (1)$$

and

$$^{36}Y(t) = \kappa(1 + x_3 k_1^{-1} + x_{-3}k_2^{-1})\{1 + A^{\beta}_{\beta}e^{-K_1 t} - B^{\beta}_{\beta}e^{-K_2 t} - (1 + A^{\beta}_{\beta} - B^{\beta}_{\beta})e^{(-k_1 k_2)t}\}, \quad (2)$$

with $\kappa = k_1k_2/K_1K_2$, and

$$x_3 = (1-e)k_3 + ek_{-3}, x_{-3} = (1-e)k_{-3} + ek_3,\ \tilde{x}_3 = x_3(k_1^{-1}+k_2^{-1}), \tilde{x}_{-3} = x_{-3}(k_1^{-1}+k_2^{-1}), \quad (3)$$

$$K_1, K_2 = \frac{1}{2}\left[k_1 + k_2 + x_3 + x_{-3} \pm \sqrt{(K_1 - k_2 - x_3 + x_{-3})^2 + 4e(x_3 - x_{-3})(k_1 - k_2) + 4x_3x_{-3}}\right],$$

$$A^{\beta}_{\alpha} = \frac{(K_1+K_2)K_2}{(k_1+k_2-K_1)(K_1-K_2)}\left[1 - \frac{K_1\{k_1(2-2e+\tilde{x}_{-3}) - K_1 + k_2\}}{(1-e)k_1(k_1+k_2)(1+\tilde{x}_{-3})}\right],$$

$$A^{\alpha}_{\beta} = \frac{(k_1+k_2)K_2}{(k_1+k_2-K_1)(K_1-K_2)}\left[1 - \frac{K_1\{k_2(2-2e+\tilde{x}_3) - K_1 + k_1\}}{(1-e)k_2(k_1+k_2)(1+\tilde{x}_3)}\right],$$

$$B^{\beta}_{\alpha} = \frac{(k_1+k_2)K_1}{(k_1+k_2-k_2)(K_1-K_2)}\left[1 - \frac{K_2\{k_1(2-2e+\tilde{x}_{-3}) - K_2 + k_2\}}{(1-e)k_1(k_1+k_2)(1+\tilde{x}_{-3})}\right],$$

$$B^{\alpha}_{\beta} = \frac{(k_1+k_2)K_1}{(k_1+k_2-k_2)(K_1-K_2)}\left[1 - \frac{K_2\{k_2(2-2e+\tilde{x}_{-3}) - K_2 + k_1\}}{(1-e)k_2(k_1+k_2)(1+\tilde{x}_{-3})}\right],$$

$$A^{\beta}_{\beta} = \frac{(k_1+k_2)K_2}{(k_1+k_2-K_1)(K_1-K_2)}\left[1 - \frac{2K_1}{k_1(1+\tilde{x}_{-3}) + k_2(1+\tilde{x}_3)}\right],$$

$$B^{\beta}_{\beta} = \frac{(k_1+k_2)K_1}{(k_1+k_2-K_2)(K_1-K_2)}\left[1 - \frac{2K_2}{k_1(1+\tilde{x}_{-3}) + k_2(1+\tilde{x}_3)}\right]. \quad (4)$$

Here, the forward- and backward-cross exchange processes are supposed to take place after the slow and fast exchange processes preceded, respectively. By the definition, k_3 is much larger than k_{-3}, because the transition state (TS) of the former must be somewhat higher in energy than that of the latter. x_3 and x_{-3} represent the mean forward-cross and backward-cross exchange rate, respectively; and K_1 and K_2 do the effective fast and slow exchange rate, respectively. In the limit of no cross-exchange, these expressions tend to those used with $e=0.12$ by Hillier and Wydrzynski (Eq. (2) in [49]).

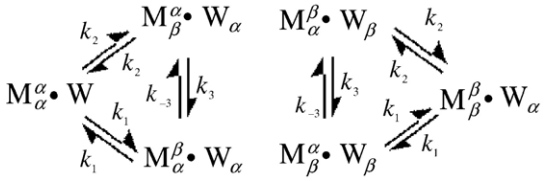

Fig. 2. A generalized scheme of the isotopic ^{18}O exchange reactions on the mono-manganese substrate binding sites in OEC: α and β stand for ^{16}O- and ^{18}O-isotope substrate; the suffix and superfix position on M implies the strong and weak binding site with the substrate exchange rates, k_1 and k_2; k_3 and k_{-3} represents the forward and backward cross exchange rates; W_{α} and W_{β} are $H_2{}^{16}O$ and $H_2{}^{18}O$; respectively.

To proof the existence of the forward cross-exchange process, we applied the statistical data analysis with the goodness-of-fit criterion [52] of Eqs. (1) and to (2) the best data in S_1-state [49], denoted $\{^{34}Y_j, t_j; j=1-N_{34}\}$ and $\{^{36}Y_k, t_k; k=1-N_{36}\}$, using the statistical χ^2 function:

$$\chi^2(\{^{34}Y, {}^{36}Y\}, \{k\}) = \sum_{j=1}^{N_{34}}\{^{34}Y_j - {}^{34}Y(t_j)\}^2/\sigma^2 + \sum_{k=1}^{N_{36}}\{^{36}Y_k - {}^{36}Y(t_k)\}^2/\sigma^2, \quad (5)$$

where the standard deviations of the experimental yields $\{^{34}Y, ^{36}Y\}$ are supposed to be evenly given by σ. This χ^2 function must take the minimum value equal to the degree of freedom $\nu = N_{34} + N_{36} - 3$ when the only three adjustable parameters, denoted $\{k\} \equiv \{k_i;\ i=1, 2, 3\}$ (k_{-3} is negligible), arrived at the most probable values $\{\bar{k}\}$, i.e. $\chi^2(\{^{34}Y, ^{36}Y\}, \{\bar{k}\}) = \nu$. This equation was used to determine $\sigma = 0.0459$ for S_1-state ($N_{34}=81$, $N_{36}=43$). In Fig. 3A, we depicted the best-fit curves to the S_1-state data points, with use of black and red colors, respectively. Then, the contour maps of the variation:

$$\Delta\chi^2 \equiv \chi^2(\{^{34}Y, {}^{36}Y\}, \{k\}) - \chi^2(\{^{34}Y, {}^{36}Y\}, \{\bar{k}\}) \quad (6)$$

at some increasing levels in (k_1, k_2) and (k_2, k_3)-space involving the minimum point at level 0 were drawn in Fig. 3B and C, respectively, to estimate the standard deviations for $\{k\}$ by using the level-1 loop. Notably, in Fig. 3B, the level-1 contour in the (k_1, k_2)-plane is a closed loop in comet-shape, which allows us to predict a large k_1 value around 400 s^{-1} despite of no data points existing below $t<4.4$ ms. This predictability is due to the cooperative consequence of the high-quality data points extending from 4.4 ms to 225 s and the generalized kinetics in Fig. 2. By the same reasons, the level-1 ellipsoid in (k_2, k_3)-plane in Fig. 3C allows us to determine a small k_3 value around 2.9×10^{-3} s^{-1} despite of no data points available above $t>225$ s. Thus, we got in S_1 state,

$$k_1 = 400 +/- 138/87\ s^{-1},$$
$$k_2 = 0.0204 \pm 0.0009\ s^{-1},$$
$$k_3 = 0.0029 \pm 0.0009\ s^{-1},\ \text{and}\ k_{-3} \ll k_3. \quad (7)$$

Significantly, the cross-exchange rate k_3 was found to be finite, clearly indicating that two substrate water molecules

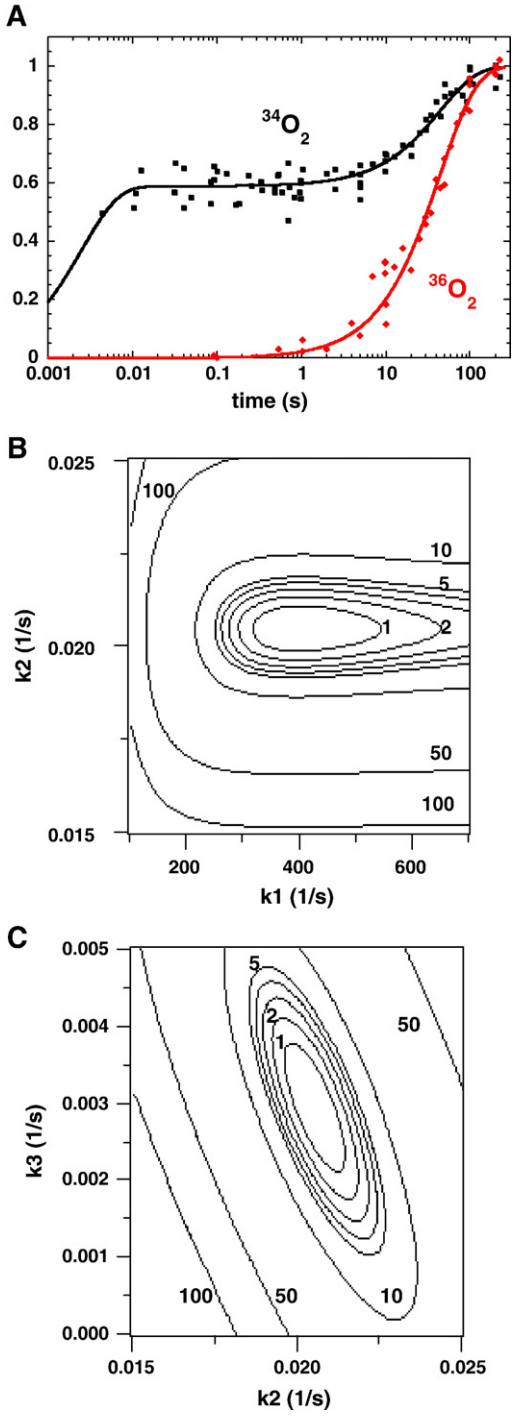

Fig. 3. (A) The least square fitting of the generalized exchange kinetics Eqs. (1) and (2) to the ^{18}O exchange data from the S_1 state sample, $^{34}O_2$ (black) and $^{36}O_2$ (red), respectively (B) and (C) the $\Delta\chi^2$ contour maps in (k_1, k_2)-plane at $k_3=2.9\times10^{-3}$ s^{-1} and (k_2, k_3)-plane at $k_1=400$ s^{-1}, respectively ($k_{-3}=0$). The forward cross exchange (k_3) from the activated transition state of the slow exchange (k_2) to that of the fast exchange (k_1) is taking place in a well-resolved 68%-probability region of $\Delta\chi^2\leq1$; $k_2=(2.04\pm\ 0.09)\times10^{-2}$, $k_3=(2.9\pm0.9)\times10^{-3}$.

must be closely bound to each other. Furthermore, the ratio of k_3/k_2 is ~0.15, a considerable value suggesting that two substrate water molecules would be bound so closely as cis-positions of the same Mn ion with somewhat different binding affinities in the Mn_4Ca cluster, rather than separately either at trans-positions on the same Mn ion or on different metallic ions (either of Mn–Mn and Mn–Ca), because in the latter models, the TS for the substrate exchange reaction in fast and slow phases must be too far separated to cross over.

Thus, the best hypothesis is that the two substrate water molecules are evidently bound at asymmetric cis-positions of the same Mn ion, with different binding affinities depending upon the S_i-state, probably not as any μ-oxo (or hydroxo) bridge. Hence, we must show that the MT-5J type Mn–Mn_3Ca cluster can be really modeled at atomic level so as to be compatible with this hypothesis as well as some related kinetic and spectroscopic data.

2.4. Amino acid residues as direct ligands

The X-ray diffraction data at 3.0–3.5 Å resolutions [6,53] reveal that 7 amino acid residues, i.e. D170, E189, H332, E333, D342, and C-terminal (A344) from D1 protein, and E354 from CP43 protein, have been assembled around the Mn_4Ca core. Since the OEC is known to be mostly susceptible to radiation damage in PSII [54], the current X-ray structures might be still reflecting photo-damaged features to some extent. In general, this type of error is prone to expand the first coordination shell owing to the disruption of μ-oxo bridges and Mn–ligand interactions, as pointed out in [8].

Interestingly, the 3.0 Å resolved X-ray structure [8] involves a very compact Mn_3 core, in coincidence with our proposal that a similarly compact Mn_3CaO_3OH cluster must exist [30,31], because four carboxylates groups provided by E189, C-terminal, CP43–E354 and D342 can be utilized as the third bridge ligand between di-μ_3-oxo bridged Mn_c–Ca, Mn_d–Ca, Mn_b–Mn_d and Mn_c–Mn_d ions, respectively, which could shorten the three Mn_i–Ca bonds ($i=b$–d) to ~3.4 Å [55] and either Mn_b–Mn_d or Mn_c–Mn_d bond to ~2.7 Å in agreement with EPR and EXAFS data. In addition, the D170, H332 and E333 residues in the Berlin model could be suitably used as a mono-dentate ligand to the terminal Mn_a, a mono-dentate ligand to Mn_c and a mono-μ_2-oxo-mono-μ_2-carboxylato bridge between Mn_a–Mn_b ions, respectively.

At first sight, the MT-5J and TDD types appear to be similarly linkable to the assigned seven protein ligands. But, our attempts of imbedding a TDD-type Mn_4Ca skeleton [36] into Berlin model met a serious difficulty, i.e. the direction of the di-μ_2-oxo bridged $Mn_a=O_2=Mn_b$ plane (which is automatically determined) obstructs the natural ligation of E333 to the Mn_a and Mn_b ions, because it is constrained as a neighbor of the H332 ligand.

2.5. Water-derivative ligands and the tautomerism in Si-states

In Fig. 4, we show the most likely MT-5J type Mn_4Ca cluster, which is coordinated by seven amino acid ligands and five oxo (or hydroxo) bridge ligands, occupying 12 and 14 coordination sites, respectively. The number of coordination sites would be 31 in total (7 from Ca), so that more 5 (=31–12–

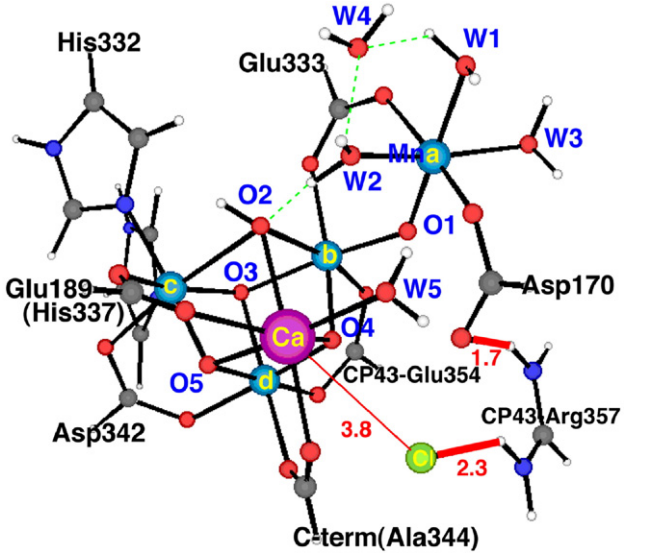

Fig. 4. A predicted structure of the OEC in the S_0 state, which consists of the most stable tautomer of the MT-5J type $Mn_4CaO_4(OH)$ cluster and its immediate vicinity to make the minimum model of enzyme field, symbolized as ClRH (or ClRH+) for cofactor Cl^- ion bound to CP43–Arg354 plus His337 (or proton-trapping His337). Atom colors are as follows: Mn, blue; Ca, magenta; Cl, green; C, grey; O, red; N, light blue; H, white. Manganese atoms are numbered from a through d, as depicted. Six water molecules involved and five oxo (or hydroxo) bridges are named W1, ●●, W5 (W6 on Ca is omitted) and O1, ●●, O5, respectively. Hydrogen bonds between W2 and O2, between W1 and W4 and between W2 and W4 are drawn by dashed lines. All residues belong to the D1 protein unless otherwise labeled.

14) sites are open for ligations by H_2O, HO^-, Cl^-, HCO_3^- ions, etc. Notably, three open sites are located on the Mn_a ion and the rest two on the Ca^{2+} ion. Furthermore, the number of positive net charges in the presumed $Mn_4(3III,IV)Ca^{2+}$ core in S_0 is 15, and these charges will be completely compensated by 15 negative charges from six carboxylates, four oxo bridges and one hydroxo bridge (the latter oxo bridges are named O1 through O5 in Fig. 4). Therefore, if the biochemical principle of charge neutrality holds in S_0, all the remaining ligands must be neutral water molecules or vacant. Since the vacant ligation is unlikely, one may suppose that the Mn_a and Ca^{2+} ions directly bind three and two water molecules, respectively. Together with a solvent water molecule that is H-bonding with two substrate water molecules, we have six functionally indispensable water molecules, denoted W1 through W6 (W6 not drawn) in Fig. 4. After all, we have arrived at the starting model of the Mn_4Ca cluster in S_0, as depicted in Fig. 4. Significantly, this model satisfies our hypothesis of mono-manganese substrate binding, so that W1 and W2 might be assigned to the fast- and slow-exchanging substrates, respectively, because W2 is tied by a H-bonding to the O2 bridge in T subunit. Notably, there is no more direct-ligation of negative ions due to the charge neutrality condition, in line with recent FTIR studies on the Cl^- binding site replaced by NO_3^- [56,57]. Similarly, a bicarbonate may not be a direct ligand to Mn in the Mn cluster [58–60].

Next, in order to investigate the tautomerism for the Mn_4Ca cluster in OEC, we have prepared four model environments; (i) gas phase, (ii) the minimum enzyme field due to charged groups and π-electron system locating nearby, (iii) the dielectric medium ($\varepsilon=4$), and (iv) the enzyme field in the dielectric medium ($\varepsilon=4$), where (iv) would be most realistic. Significantly, only two tautomers were found to be thermally distributable in the S_0 state (the other tautomers are much more unstable), designated S_{0a} and S_{0b}, which are mutually convertible by proton transfer (PT) between W3 and O1, as shown in Table 1.

Notably, this problem is deeply related with a long-standing mystery, i.e. where and when four protons are released from the M_4Ca cluster after Y_Z oxidized by $P680^+$ during a Kok's cycle. A widely-accepted view is that the intrinsic proton release pattern at physiological pH would be 1:0:1:2 [38,39]. Furthermore, the recent X-ray structures [6,8] are consistent with the idea that a phenolic proton of the oxidized $Y_Z^{+\bullet}$ could be only shifted to the H190 side along the hydrogen-bond between them [61,62]. Therefore, the 1st proton must be released from the Mn_4Ca cluster in S_0 directly into Lamella phase, in agreement with our DFT calculation of the energy difference (261.9 kcal/mol) between the oxidized state (S_{1b}^+) and its proton-released state (S_{1b}), which is just balanced with the hydration energy of a proton, 261 kcal/mol. However, upon the S_1 to S_2 transition, the 2nd proton must stay in the Mn_4Ca cluster (keeping S_{2j}^+) or transfer to some acidic group nearby (relaxing into S_{2j}). Anyway, this proton will be released just after Y_Z was oxidized, which may be just before the S_2 to S_3 transition. As for the 3rd proton, the similar processes will be met.

To elucidate this problem, we could not avoid modeling for a binding site of cofactor Cl^- and a trapping site of a released proton. Fortunately, this modeling could be unambiguously achieved by virtue of the recent X-ray structures [6,8]. By means of molecular mechanics (MM) simulations, we found out a deepest potential valley with a rather wide bottom between two amide groups of CP43-R357 and Ca^{2+} ion, as shown in Fig. 4. The functional role of Cl^- would be therefore to compensate the positive charge of CP43–R357, which has had no more counter charge group of Asp or Glu residue nearby, because too many (already six) carboxylates together with CP43–E354 have been used to form the redox active Mn_4Ca cluster. In Fig. 4, it should be noted that the Cl^- ion is bound to a hydrogen atom of one amide group at distance of ~2.3 Å, rather than to Ca^{2+} ion at distance of ~3.8 Å. This is because the Ca ion is already coordinated by seven ligands with an excessive negative charge in total. Thus, the present OEC model is completely in line with the FTIR data [56,57]. In addition, our finding that two amide groups of CP43–R357 provide a rather wide potential valley for a negative ion appears to explain why Cl^- ion is invisible in X-ray diffraction experiment. Furthermore, the recent X-ray structures [6,8] and our own DFT calculations indicate that H337 may be serving as the nearest proton-trapping site. Thus, we modeled the minimum enzyme field as consisting of Cl^- ion bound to CP43–R357 and H337 (or its proton-trapping state), symbolized as ClRH (or $ClRH^+$).

Applying this model to the S_2-state, we found that a concerted PT from the S_{2a}^+–Mn_4Ca cluster to H337 can energetically take place if any surrounding H-bond network is available, because this reaction is slightly exothermic ($\Delta\Delta E_\varepsilon$= −5.5 to −4.3 kcal/mol, see Table 1). Then, the Mn_4Ca cluster in

Table 1
Physical and chemical natures of a few tautomers of the MT-5J type Mn_4Ca cluster in OEC, which may be thermally or chemically activated in each S-state by intra-cluster proton transfer between five water-derivative ligands around the terminal Mn_a ion (see Fig. 4)

[a]S_{ij}-state /+	Water-derivative ligands					[b]$\Delta\Delta E_1$	[b]$\Delta\Delta E_4$	[c]$R_{ab}/R_{bc}/R_{bd}/R_{cd}$	4 Mn valences
Enzyme Field	W1	W2	W3	O1	O2	$\varepsilon=1$	$\varepsilon=4$	$R_{be}/R_{ce}/R_{de}$ (Å)	[d]Spins:$S_a/S_b/S_c/S_d$
S_{0a}/+ClRH	H_2O	H_2O	HO^-	HO^-	HO^-	−9.6 / 2.0	−6.9 / 3.5	3.61/3.35/2.78/2.74 3.26/3.48/3.26	III, III, III, IV 1.95/1.96/1.95/1.52
S_{0b}/+ClRH	H_2O	H_2O	H_2O	O^{2-}	HO^-	0 / 0	0 / 0	3.26/3.33/2.76/2.75 3.57/3.32/3.24	III, III, III, IV 1.95/1.96/1.95/1.52
S_{1a}/+ClRH	HO^-	H_2O	HO^-	HO^-	HO^-	−2.6/−3.3	−0.3/−0.1	3.58/3.13/2.74/2.76 3.36/3.39/3.29	IV, III, III, IV 1.54/1.92/1.97/1.52
S_{1b}/+ClRH	H_2O	HO^-	H_2O	O^{2-}	HO^-	0 / 0	0 / 0	3.37/3.16/2.76/2.76 3.38/3.30/3.27	IV, III, III, IV 1.39/1.94/1.96/1.52
S^+_{2b}/+ClRH	HO^-	HO^-	H_2O	HO^-	HO^-	251/ 5.5	274/4.3	3.32/3.22/2.76/2.82 3.40/3.48/3.31	IV, III, III, IV 1.40/1.51/1.96/1.50
S_{2a}/+ClRH$^+$	HO^-	HO^-	HO^-	HO^-	HO^-	−3.4/−2.6	−2.6/−5.3	3.55/3.11/2.74/2.77 3.34/3.40/3.28	IV, IV, III, IV 1.48/1.51/1.96/1.51
S_{2b}/+ClRH$^+$	HO^-	HO^-	H_2O	O^{2-}	HO^-	0 / 0	0 / 0	3.31/3.17/2.76/2.75 3.34/3.39/3.27	IV, IV, III, IV 1.46/1.47/1.96/1.51
S_{2c}/+ClRH$^+$	HO^-	H_2O	H_2O	O^{2-}	O^{2-}	−3.8/ 24.6	−2.1/ 23.3	3.30/2.88/2.78/2.70 3.27/3.31/3.31	III, IV, IV, IV 1.95/1.44/1.50/1.49
S^+_{3a}/+ClRH	HO^-	HO^-	HO^-	HO^-	HO^-	−5.7 /−5.7	5.3 /6.7	3.56/2.84/2.74/2.74 3.32/3.34/3.33	IV, IV, IV, IV 1.47/1.50/1.49/1.49
S^+_{3b}/+ClRH	HO^-	HO^-	H_2O	O^{2-}	HO^-	0 / 0	0 / 0	3.30/3.00/2.77/2.72 3.44/3.39/3.30	IV, IV, IV, IV 1.47/1.43/1.49/1.49
S^+_{3c}/+ClRH	HO^-	H_2O	H_2O	O^{2-}	O^{2-}	5.0 / 1.5	35 / 39	3.45/2.84/2.74/2.74 3.41/3.34/3.33	IV, IV, IV, IV 1.41/1.47/1.50/1.49
S_{3b}/+ClRH$^+$	HO^-	HO^-	HO^-	O^{2-}	HO^-	290 /50	307 /35	3.33/2.89/2.78/2.70 3.28/3.28/3.29	IV, IV, IV, IV 1.48/1.37/1.50/1.49

[a] "S_{ij}" represents the "j" labeled tautomer in S_i-state, ClRH symbolizes the minimum enzyme field consisting of Cl^- ion bound to CP43–R357 and H337, and ClRH$^+$ is used for ClRH with a protonated H337.
[b] Four $\Delta\Delta E_\varepsilon$'s of each tautomer in the same S_i-state (i=0–3) are the relative energies to the underlined states (ε=1, 4; in units of kcal/mol).
[c] R_{mn} (m=a–d) are the predicted distances between Mn_m and Mn_n ions for n=a–d and between Mn_m and Ca ions for n=e.
[d] S_m is a half of the Muliken spin population on Mn_m ion.

S_2 must become neutral and the 2nd proton may be trapped at H337. In contrast, the PT reaction from the S^+_{3b}–Mn_4Ca cluster to H337 was found to be highly endothermic ($\Delta\Delta E_\varepsilon$=50–35 kcal/mol in Table 1), indicating that the Mn_4Ca cluster in S_3 must keep the 3rd proton unreleased, having a positive charge in S^+_{3j} tautomers$^+$(j=a, b).

We have summarized the physical and chemical natures of thermally distributable tautomers of the MT-5J type Mn_4Ca cluster in four Kok's S_i-states; i=0–3, in Table 1, and also the predicted substrate–water-binding states in the dominant tautomers, i.e. S_{ib}-states (i=0–3), together with the calculated fast and slow substrate exchange rates, in Table 2. Some fundamental results picked up here will be discussed in comparison with related experimental data in the following.

3. Discussions

3.1. The tautomerism and substrate binding states in Kok S_i-states

In the MT-5J type Mn_4Ca cluster, the tautomerism can take place between H-bonding neighbors, i.e. (W3, O1) and (W2, O2), showing water-oxy(WO), water-hydroxy(WH), hydroxy-hydroxy (HH) and hydroxy-oxy(HO) tautomers in Table 1 (see W2, W3, O1, O2 rows). The S_{ia}-states (i=0–3) are characterized by the common HH tautomer in the (W3, O1) pair, while the other S_{ij}(except for S_{3b})-states by the common WO tautomer in this pair. On the basis of the calculated relative energies $\Delta\Delta E_\varepsilon$'s in Table 1 and the environmental volume-exclusion effect of the mono-μ-hydroxo bridged M and T subunits being more expanded than the mono-μ-oxo bridged one (compare their R_{ab} distances in Table 1), one may assume that the S_{ib}(S^+_{3b} in S_3)-state tautomer might be most stable in each S_i state. In fact, the molecular structures of these tautomers show an amazing correlation between the S-state dependences of the substrate water binding states and the observed ^{18}O exchange rates in fast and slow phases [42], as summarized in Table 2. Such an amazing correlation like this was not found for the S_{ia} tautomers (not shown).

First of all, our results in Table 2 indicate that the substrate exchange rate depends on many factors: (i) the species of the substrate, H_2O or HO^-, (ii) the oxidation state of the metal ion, (iii) the coordination site relative to the mono-μ-oxo bridge, (iv) the metal–substrate bond length,

Table 2
Correlated S-state dependences between two substrate water exchange rates (k_1, k_2) and their monomeric binding states for the MT-5J type Mn_a–Mn_3Ca cluster[a] in OEC

	S_{0b} state	S_{1b} state	S_{2b} state	S^+_{3b} state
Valence of Mn_a	III	IV	IV	IV
W1/W2/O2	$H_2O/H_2O/HO^-$	$H_2O/HO^-/HO^-$	$HO^-/HO^-/HO^-$	$HO^-/HO^-/HO^-$
k_1 [b]/s^{-1}	>1100	400+/−138/87	126±7	37.2±1.2
d(Mn_a-W1)/Å	2.178	2.192	1.831	1.789
k_2 [b]/s^{-1}	13.8±1.5	0.0204±0.0009	2.01±0.09	2.02±0.06
d(Mn_a-W2)/Å	2.211	1.836	1.870	1.868
d(W2-O2)/Å	2.451	3.100	2.711	2.711

[a] Dominant stable tautomer of this cluster must be S_{jb} (j=0–3) (see Table 1).
[b] These experimental values were obtained in the same way as described in Section 2.3.

and (v) the existence of H-bonding. The fact that the S_2 and S_3 state samples show amazingly similar substrate water exchange rates (k_1, k_2) can be readily explained in terms of our theoretical predictions showing that the above four factors are almost identical between the S_{2b} and S^+_{3b} states. Even a predicted small difference of the Mn_a(IV)–O(W1) bond length, 1.831 Å (S_{2b}) vs. 1.789 Å (S^+_{3b}), appears to be consistent with the observed difference of k_1, 126 s^{-1} (S_2) vs. 37 s^{-1} (S_3). It is noteworthy that the substrate W2 must yield a much smaller exchange rate than the substrate W1 in these S-states, despite of the d(Mn_a(IV)–W2) being longer than the d(Mn_a(IV)–W1). This phenomenon can be explained in terms of the existence of a strong H-bonding between W2 and O2, which will elongate the Mn_a(IV)–W2 bond length. In contrast, in the S_{1b} state, this H-bonding appears to be much weaker than in the S_{2b} and S^+_{3b} states, and hence the bond length d(Mn_a(IV)–W2) is the shortest (1.836 Å), indicating that the k_2 can take the smallest value, 2.0×10^{-2} s^{-1}. On the other hand, the predicted fast exchange rate ~400 s^{-1} can be interpreted in terms of the largest bond length of d(Mn_a(IV)–W1)=2.192 Å. The difference between substrates, H_2O and HO^-, can become one of the important factors to affect the exchange rate. The predicted large bond lengths for the substrate H_2O in S_{0b} and S_{1b} states show a good correspondence to unresolvably high exchange rates. Furthermore, the observed slow exchange rate in S_0 state (13.8 s^{-1}) would be mainly due to the predicted very strong H-bonding between substrate H_2O and O2 bridge (2.451 Å).

Recently, it was reported that, upon replacement of Ca^{2+} with Sr^{2+}, the k_2 increases by a factor of 3–4 across the S_1, S_2, and S_3 states, but then k_1 in S_3 appears to be affected little, while k_1's in S_0 and S_1 remain largely unresolvable [63]. This finding seems to support a part of the predicted structure of the present MT-5J type Mn_4Ca cluster around the Ca^{2+} ion, which binds two water molecules, one of them (i.e. W6; not shown in Fig. 4) being used as the shortest ET pathway to $Y^{\bullet}_Z$ radical and the other (i.e. W5) used as a middle water molecule in a H-bonded ET bypath, i.e. W1(Mn_a)W2–W5–W6–$Y^{\bullet}_Z$.

3.2. Oxidation state change

The valence state of each Mn_4Ca cluster can be self-consistently determined as shown in the last line in Table 1; i.e.. S_{0b}(III,III,III,IV), S_{1b}(IV,III,III,IV), S_{2b}(IV,IV,III,IV) and S_{3b}(IV,IV,IV,IV), in consistent with our early Mn K-edge XAFS data [11,12]. In this model, only Mn_d ion keeps valence IV through a Kok cycle, but Mn_a, which binds Asp170, takes valence III only in S_0 and valence IV in S_1 through S_3. But, a recent FTIR data from D170H mutation [64] shows that the oxidation of the Mn_4Ca cluster does not induce any detectable frequency shift around the region of carboxylate stretching modes during the successive S-state transitions. Our interpretation for this phenomenon is like that the carboxylate stretching mode of Asp170 may be too diffusive and/or too over-dumping to make it detectable, because Asp170 indeed interacts with heterogeneous groups involving O1, W1, Ca^{2+} and Cl^- ions, Asp61, CP43–Arg357 and surrounding water molecules.

3.3. The predicted skeleton structures and EXAFS

As seen from the 9th row (R_{ij}) in Table 1, the S_{1b} and S_{2b} states similarly contain two groups of Mn–Mn distances, i.e. ~2.755±0.005 Å and ~3.27±0.10 Å, and one group of Mn–Ca distances, i.e. 3.27–3.38 Å, in good agreements with the very similar Mn K-edge [26,65,66] and Ca K-edge [55] EXAFS data. In contrast, the S^+_{3b} state shows significantly heterogeneous Mn–Mn distances at 2.72, 2.77, 3.00 and 3.30 Å and relatively uniform Mn–Ca distances at 3.44, 3.39 and 3.30 Å, consistently with the split and upshifted experimental distribution [67]. However, the EXAFS data from S_0 state [68] show some discrepancy from the predicted structures of the S_{0a} and S_{0b} tautomers.

4. Conclusions

To elucidate the structure of the oxygen-evolving complex (OEC) involving the catalytic Mn_4Ca cluster, we have investigated many possible model structures of the Mn_4Ca(Cl) cluster by means of DFT/B3LYP geometry optimizations, critically finding out a unique most-likely model, that is a monomer–trimer (MT) type of the Mn–$Mn_3CaO_{5-x}(HO)_x$ cluster compactly ligated by six carboxylate groups and an imidazole group from amino acids in photosystem II (PSII). In this model, the structure of the ligating amino acid residues is remarkably kept close to the original X-ray crystallographic model [8]. Next, to abstract the precise information on the nature of the binding sites for two substrate water molecules in OEC from the most reliable S_1-state data, we have expanded the theory of ^{18}O exchange reaction kinetics so as to involve the asymmetric cross exchange pathways between the transition states in slow and fast exchange processes. Contrary to a common view (i.e. independent binding sites), the ratio of the resolved cross exchange rate to the slow one taking a considerable value of ~0.15 reveals that two substrate water molecules are most probably bound to asymmetric cis-positions on the same Mn ion as terminal ligands: the slowly-exchangeable one may be tied by intra-(Mn_4Ca)cluster hydrogen bond(s). These findings and the charge neutrality principle in biochemistry led us to a complete modeling of the most-likely MT-type $Mn_4CaO_4(OH)$ cluster in S_0-state, leaving the freedom of the tautomerism, unknown binding sites of cofactor Cl^- and a bicarbonate, and a trapping site of released protons near the Mn_4Ca cluster. We have carried out the molecular mechanics search for the most stable position of Cl^- ion in OEC to find it out between CP43–Arg357 and Ca^{2+} ion, suggesting the functional role is to compensate the positive charge of the Arg, and also the DFT search for physiologically important tautomers of the Mn_4Ca cluster in each S_i-state (i=0–3) to characterize their physical and chemical natures in four kinds of the model enzyme field, providing most reasonable interpretations for directly related kinetic and spectroscopic (EPR, XAFS and EXAFS) data. The predicted structures of the unique MT-5J

type Mn_4Ca clusters (the most stable tautomer in each S_i-state; $i=1–3$) revealed that two substrate water molecules on the terminal Mn ion are bound in such a way as completely consistent with the S-state dependence of observed fast and slow ^{18}O exchange rates.

Acknowledgment

We thank Prof. Tom Wydrzynskii for sending us digital data of ^{18}O exchange kinetics to be used for the present theoretical analysis.

References

[1] B. Kok, B. Forbush, M. McGloin, Cooperation of charges in photosynthetic O_2 evolution-I. A linear four step mechanism, Photochem. Photobiol. 11 (1970) 457–475.
[2] R.J. Debus, The manganese and calcium ions of photosynthetic oxygen evolution, Biochim. Biophys. Acta 1102 (1992) 269–352.
[3] G. Renger, Coupling of electron and proton transfer in oxidative water cleavage in photosynthesis, Biochim. Biophys. Acta 1655 (2004) 195–204.
[4] A. Zouni, H.T. Witt, J. Kern, P. Fromme, N. Krauss, W. Saenger, P. Orth, Crystal structure of photosystem II from *Synechococcus elongatus* at 3.8 Å resolution, Nature 409 (2001) 739–743.
[5] N. Kamiya, J.-R. Shen, Crystal structure of oxygen-evolving photosystem II from *Thermosynechococcus vulcanus* at 3.7-Å resolution, Proc. Natl. Acad. Sci. U. S. A. 100 (2003) 98–103.
[6] K.N. Ferreira, T.M. Iverson, K. Maghlaoui, J. Barber, S. Iwata, Architecture of the photosynthetic oxygen-evolving center, Science 303 (2004) 1831–1838.
[7] J. Kern, B. Loll, A. Zouni, W. Saenger, K.-D. Irrgang, J. Biesiadka, Cyanobacterial photosystem II at 3.2 Å resolution — the plastoquinone binding pockets, Photosynth. Res. 84 (2005) 153–159.
[8] B. Loll, J. Kern, W. Saenger, A. Zouni, J. Biesiadka, Towards complete cofactor arrangement in the 3.0 Å resolution structure of photosystem II, Nature 438 (2005) 1040–1044.
[9] P.E. Siegbahn, M. Lundberg, The mechanism for dioxygen formation in PSII studied by quantum chemical methods, Photochem. Photobiol. Sci. 4 (2005) 1035–1043.
[10] J.P. McEvoy, J.A. Gascon, V.S. Batista, G.W. Brudvig, The mechanism of photosynthetic water splitting, Photochem. Photobiol. Sci. 4 (2005) 940–949.
[11] T. Ono, T. Noguchi, Y. Inoue, M. Kusunoki, T. Matsushita, H. Oyanagi, X-ray detection of the period-four cycling of the manganese cluster in photosynthetic water oxidizing enzyme, Science 258 (1992) 1335–1337.
[12] M. Kusunoki, T. Ono, T. Noguchi, Y. Inoue, H. Oyanagi, Manganese K-edge X-ray absorption spectra of the cyclic Kok's S-states in the photosynthetic oxygen-evolving system, Photosynth. Res. 38 (1993) 331–339.
[13] V.K. Yachandra, V.J. DeRose, L. Matthew, I. Mukerji, K. Sauer, M.P. Klein, Where plants make oxygen: a structural model for the photosynthetic oxygen-evolving manganese cluster, Science 260 (1993) 675–679.
[14] W. Liang, M.J. Latimer, H. Dau, T.A. Roelofs, V.K. Yachandra, K. Sauer, M.P. Klein, Correlation between structure and magnetic spin state of the manganese cluster in the oxygen-evolving complex of photosystem II in the S_2 state: determination by X-ray absorption spectroscopy, Biochemistry 33 (1994) 4923–4932.
[15] V.K. Yachandra, Structure of the manganese complex in photosystem II: insights from X-ray spectroscopy, Philos. Trans. R. Soc. Lond., B 357 (2002) 1347–1357.
[16] H. Dau, P. Liebisch, M. Haumann, The structure of the manganese complex of Photosystem II in its dark-stable S_1-state EXAFS results in relation to recent crystallographic data, Phys. Chem. Chem. Phys. 6 (2004) 4781–4792.
[17] M. Haumann, C. Müller, P. Liebisch, L. Iuzzolino, J. Dittmer, M. Grabolle, T. Neisius, W. Meyer-Klaucke, H. Dau, Structural and oxidation state changes of the photosystem II manganese complex in four transitions of the water oxidation cycle ($S(0)\rightarrow S(1)$, $S(1)\rightarrow S(2)$, $S(2)\rightarrow S(3)$, and $S(3,4)\rightarrow S(0)$) characterized by X-ray absorption spectroscopy at 20 K and room temperature, Biochemistry 44 (2005) 1894–1908.
[18] J.L. Casey, K. Sauer, EPR detection of a cryogenically photogenerated intermediate in photosynthetic oxygen evolution, Biochim. Biophys. Acta 767 (1984) 21–28.
[19] J.-L. Zimmermann, A.W. Rutherford, EPR studies of the oxygen-evolving enzyme of Photosystem II, Biochim. Biophys. Acta 767 (1984) 160–167.
[20] J. Messinger, J. Robblee, W.O. Yu, K. Sauer, V.K. Yachandra, M.P. Klein, The S_0 state of the oxygen-evolving complex in Photosystem II is paramagnetic: detection of an EPR multiline signal, J. Am. Chem. Soc. 119 (1997) 11349–11350.
[21] K.A. Åhrling, S. Peterson, S. Styring, An oscillating manganese electron paramagnetic resonance signal from the S_0 state of the oxygen evolving complex in photosystem II, Biochemistry 36 (1997) 13148–13152.
[22] T. Yamauchi, H. Mino, T. Matsukawa, A. Kawamori, T. Ono, Parallel polarization electron paramagnetic resonance studies of the S_1-state manganese cluster in the photosynthetic oxygen-evolving system, Biochemistry 36 (1997) 7520–7526.
[23] K.A. Campbell, J.M. Peloquin, D.P. Pham, R.J. Debus, R.D. Britt, Parallel polarization EPR detection of an S_1-state 'multiline' EPR signal in photosystem II particles from *Synechocystis* sp. PCC 6803, J. Am. Chem. Soc. 120 (1998) 447–448.
[24] T. Matsukawa, H. Mino, D. Yoneda, A. Kawamori, Dual-mode EPR study of new signals from the S_3-state of oxygen-evolving complex in photosystem II, Biochemistry 38 (1999) 4072–4077.
[25] G.N. George, R.C. Prince, S.P. Cramer, The manganese site of photosynthetic water-splitting enzyme, Science 243 (1989) 789–791.
[26] V.K. Yachandra, R.D. Guiles, A.E. McDermott, J.L. Cole, R.D. Britt, S.L. Dexheimer, K. Sauer, M.P. Klein, Comparison of the structure of the manganese complex in the S_1 and S_2 states of the photosynthetic O_2-evolving complex: an X-ray absorption spectroscopy study, Biochemistry 26 (1987) 5974–5981.
[27] M.P. Klein, K. Sauer, V.K. Yachandra, Perspectives on the structure of the photosynthetic oxygen evolving manganese complex and its relation to the Kok cycle, Photosynth. Res. 38 (1993) 265–277.
[28] M. Kusunoki, A new paramagnetic hyperfine structure effect in manganese tetramers. The origin of "multiline" EPR signals from an S_2 state of a photosynthetic water-splitting enzyme, Chem. Phys. Lett. 197 (1992) 108–116.
[29] K. Hasegawa, M. Kusunoki, Y. Inoue, T.A. Ono, Simulation of S_2-state multiline EPR signal in oriented photosystem II membranes: structural implications for the manganese cluster in an oxygen-evolving complex, Biochemistry 37 (1998) 9457–9465.
[30] K. Hasegawa, T. Ono, Y. Inoue, M. Kusunoki, Spin–exchange interactions in the S_2-state manganese tetramer in photosynthetic oxygen-evolving complex deduced from $g=2$ multiline EPR signal, Chem. Phys. Lett. 300 (1999) 9–19.
[31] K. Hasegawa, T. Ono, Y. Inoue, M. Kusunoki, How to evaluate the structure of a tetranuclear Mn cluster from magnetic and EXAFS data: case of the S_2-State Mn-cluster in Photosystem II, Bull. Chem. Soc. Jpn 72 (1999) 1013–1023.
[32] J.M. Peloquin, R.D. Britt, EPR/ENDOR characterization of the physical and electronic structure of the OEC Mn cluster, Biochim. Biophys. Acta 1503 (2001) 96–111.
[33] M. Kusunoki, Simulation of the "S_0-state" EPR signal from the Mn cluster in photosystem II, Evidence for a piece of a thermally accessible O_2-binding state, Proc. 12th Int. Congr. Photosynthesis, Csiro publishing, Collingwood, Australia, 2001, pp. S13–S008.
[34] M. Kusunoki, A Consistent Special Arrangement of Spins of the Manganese Cluster and a Tyrosine Radical $Yz^{\bullet}$ in the Oxygen Evolving Center in Photosystem II, in: G. Garab (Ed.), Photosynthesis: Mechanisms and Effects, vol. II, Kluwer Academic, Dordrecht, 1998, pp. 1371–1374.

[35] Y. Komatsuzaki, M. Kusunoki, Highly structure-sensitive EXAFS spectra from multinuclear Mn model compounds, Ab initio refinement of a diamond-structure of the S_1-state MnCaCl cluster in photosystem II, Proc. 12th Int. Congr. Photosynthesis, Csiro publishing, Collingwood, Australia, 2001, pp. S13–S012.
[36] M. Kusunoki, Mechanism of the Photosynthetic Water Oxidation Reaction Catalyzed By A Noble Mn_4CaCl-Bicarbonate Cluster, in: D. Bruce, A. van der Est (Eds.), Photosynthesis: Fundamental Aspects to Global Perspectives, vol. 1, Allen Press, Lawrence, 2005, pp. 410–412.
[37] J. Yano, J. Kern, K. Sauer, M.L. Latimer, Y. Puchkar, J. Biesaidka, B. Loll, W. Saenger, J. Messinger, A. Zouni, V.K. Yachandra, Where water is oxidized to dioxygen: structure of the photosynthetic Mn_4Ca cluster, Science 314 (2006) 821–824.
[38] M. Haumann, W. Junge, Extent and rate of proton release by photosynthetic water oxidation in thylakoids: electrostatic relaxation versus chemical production, Biochemistry 33 (1994) 864–872.
[39] E. Schlödder, H.T. Witt, Stoichiometry of proton release from the catalytic center in photosynthetic water cleavages in photosynthetic water oxidation. Re-examination by a glass electrode study at pH 5.5–7.2, J. Biol. Chem. 274 (1999) 30387–30392.
[40] M.C. Evans, J.H. Nugent, R.J. Ball, I. Muhiuddin, R.J. Pace, Evidence for a direct manganese–oxygen ligand in water binding to the S_2 state of the photosynthetic water oxidation complex, Biochemistry 43 (2004) 989–994.
[41] R.D. Britt, K.A. Campbell, J.M. Peloquin, M.L. Gilchrist, C.P. Aznar, M. M. Dicus, J. Robblee, J. Messinger, Recent pulsed EPR studies of the Photosystem II oxygen-evolving complex: implications as to water oxidation mechanisms, Biochim. Biophys. Acta 1655 (2004) 158–171.
[42] W. Hillier, T. Wydrzynski, Substrate water interactions within the photosystem II oxygen evolving complex, Phys. Chem. Chem. Phys. 6 (2004) 4882–4889.
[43] T. Noguchi, M. Sugiura, FTIR detection of water reactions during the flash-induced S-state cycle of the photosynthetic water-oxidizing complex, Biochemistry 41 (2002) 15706–15712.
[44] A. Kimura, A. Ishii, T. Yamanari, T. Ono, Water-sensitive low-frequency vibrations of reaction intermediates during S-state cycling in photosynthetic water oxidation, Biochemistry 44 (2005) 7613–7622.
[45] E.M. Sproviero, J.A. Gascon, J.P. McEvoy, G. Brudvig, V.S. Batista, Characterization of synthetic oxomanganese complexes and the inorganic core of the O_2-evolving complex in photosystem II: evaluation of the DFT/B3LYP level of theory, J. Inorg. Biochem. 100 (2006) 786–800.
[46] Jaguar5.1, vol. Schrödinger, L.L.C., Portland, OR, 1991–2003.
[47] T.A. Roelofs, W. Liang, M.J. Latimer, R.M. Cinco, A. Rompel, J.C. Andrews, K. Sauer, V.K. Yachandra, M.P. Klein, Oxidation states of the manganese cluster during the flash-induced S-state cycle of the photosynthetic oxygen-evolving complex, Proc. Natl. Acad. Sci. U. S. A. 93 (1996) 3335–3340.
[48] D. Kuzek, R.J. Pace, Probing the Mn oxidation states in the OEC. Insights from spectroscopic, computational and kinetic data, Biochim. Biophys. Acta 1503 (2001) 123–137.
[49] W. Hillier, T. Wydrzynski, Oxygen ligand exchange at metal sites — implications for the O_2 evolving mechanism of photosystem II, Biochim. Biophys. Acta 1503 (2001) 197–209.
[50] M. Zheng, G.C. Dismukes, Orbital configuration of the valence electrons, ligand field symmetry, and manganese oxidation states of the photosynthetic water oxidizing complex: analysis of the S_2 state multiline EPR signals, Inorg. Chem. 35 (1996) 3307–3319.
[51] J. Messinger, J.H. Robblee, U. Bergmann, C. Fernandez, P. Glatzel, H. Visser, R.M. Cinco, K.L. McFarlane, E. Bellacchio, S.A. Pizarro, S.P. Cramer, K. Sauer, M.P. Klein, V.K. Yachandra, Absence of Mn-centered oxidation in the S_2–S_3 transition: implications for the mechanism of photosynthetic water oxidation, J. Am. Chem. Soc. 123 (2001) 7804–7820.
[52] P.R. Bevington, Data Reduction and Error Analysis for the Physical Sciences, McGraw-Hill, New York, 1969, pp. 66–91.
[53] J. Barber, Structural model of the oxygen-evolving center of photosystem II with mechanistic implications, Phys. Chem. Chem. Phys. 6 (2004) 4737–4742.
[54] J. Yano, J. Kern, K.-D. Irrgang, M.J. Latimer, U. Bergmann, P. Glatzel, Y. Pushkar, J. Biesiadka, B. Loll, K. Sauer, J. Messinger, A. Zouni, V.K. Yachandra, X-ray damage to the Mn4Ca complex in single crystals of photosystem II: a case study for metalloprotein crystallography, Proc. Natl. Acad. Sci. U. S. A. 102 (2005) 12047–12052.
[55] R.M. Cinco, H. McFarlane, J.H. Robblee, J. Yano, S.A. Pizarro, E. Bellacchio, K. Sauer, V.K. Yachandra, Calcium EXAFS establishes the Mn–Ca cluster in the oxygen-evolving complex of photosystem II, Biochemistry 41 (2002) 12928–12933.
[56] K. Hasegawa, Y. Kimura, T.-a. Ono, Chloride cofactor in the photosynthetic oxygen-evolving complex studied by Fourier transform infrared spectroscopy, Biochemistry 41 (2000) 13839–13850.
[57] K. Hasegawa, Y. Kimura, T.A. Ono, Oxidation of the Mn cluster induces structural changes of NO_3-functionally bound to the Cl-site in the oxygen-evolving complex of photosystem II, Biophys. J. 86 (2004) 1042–1050.
[58] S.V. Baranov, A.M. Tyryshkin, D. Katz, G.C. Dismukes, G.M. Ananyev, V.V. Klimov, Bicarbonate is a native cofactor for assembly of the manganese cluster of the photosynthetic water oxidizing complex. Kinetics of reconstitution of O_2 evolution by photoactivation, Biochemistry 43 (2004) 2070–2079.
[59] D.N. Shevela, A.A. Khorobrykh, V.V. Klimov, Effect of bicarbonate on the water-oxidizing complex of photosystem II in the super-reduced S-states, Biochim. Biophys. Acta 1757 (2006) 253–261.
[60] P.E. Siegbahn, M. Lundberg, Hydroxide instead of bicarbonate in the structure of the oxygen evolving complex, J. Inorg. Biochem. 100 (2006) 1035–1040.
[61] F. Mamedov, R.T. Sayre, S. Styring, Involvement of histidine 190 on the D1 protein in electron/proton transfer reactions on the donor side of photosystem II, Biochemistry 37 (1998) 14245–14256.
[62] A.M. Hays, I.R. Vassiliev, J.H. Golbeck, R.J. Debus, Role of D1-His190 in proton-coupled electron transfer reactions in photosystem II: a chemical complementation study, Biochemistry 37 (1998) 11352–11365.
[63] G. Hendry, T. Wydrzynski, (18)O isotope exchange measurements reveal that calcium is involved in the binding of one substrate–water molecule to the oxygen-evolving complex in photosystem II, Biochemistry 42 (2003) 6209–6217.
[64] R.J. Debus, M.A. Strickler, L.M. Walker, W. Hillier, No evidence from FTIR difference spectroscopy that aspartate-170 of the D1 polypeptide ligates a manganese ion that undergoes oxidation during the S(0) to S(1), S (1) to S(2), or S(2) to S(3) transitions in photosystem II, Biochemistry 44 (2005) 1367–1374.
[65] D.J. MacLachlan, B.J. Hallahan, S.V. Ruffle, J.H.A. Nugent, M.C.W. Evans, R.W. Strange, S.S. Hasnain, An e.x.a.f.s. study of the manganese O_2-evolving complex in purified Photosystem II membrane fractions. The S_1 and S_2 states, Biochem. J. 285 (1992) 569–576.
[66] V.J. DeRose, I. Mukerji, M.J. Latimer, V.K. Yachandra, K. Sauer, M.P. Klein, Comparison of the manganese oxygen-evolving complex in photosystem II of spinach and *Synechococcus* sp. with multinuclear manganese model compounds by X-ray absorption spectroscopy, J. Am. Chem. Soc. 116 (1994) 5239–5249.
[67] W. Liang, T.A. Roelofs, R.M. Cinco, A. Ronpel, M.J. Latimer, W.O. Yu, K. Sauer, M.P. Klein, V.K. Yachandra, Structural change of the Mn cluster during the $S_2 \rightarrow S_3$ state transition of the oxygen-evolving complex of photosystem II. Does it reflect the onset of water/substrate oxidation? Determination by Mn X-ray absorption spectroscopy, J. Am. Chem. Soc. 122 (2000) 3399–3412.
[68] J.H. Robblee, J. Messinger, R.M. Cinco, K.L. McFarlane, C. Fernandez, S.A. Pizarro, K. Sauer, V.K. Yachandra, The Mn cluster in the S(0) state of the oxygen-evolving complex of photosystem II studied by EXAFS spectroscopy: are there three Di-μ-oxo-bridged Mn(2) moieties in the tetranuclear Mn complex? J. Am. Chem. Soc. 124 (2002) 7459–7471.